physics

IMPACT FACTOR 1.8

CITESCORE 3.1

Article

Reinterpretation of Fermi Acceleration of Cosmic Rays in Terms of Ballistic Surfing Acceleration in Supernova Shocks

Krzysztof Stasiewicz

Special Issue

A Themed Issue in Honor of Professor Lennart Stenflo on the Occasion of His 85th Birthday: Plasma Physics and Nonlinear Science

Edited by

Prof. Gert Brodin and Prof. Dr. Hans László Pécseli

MDPI

https://doi.org/10.3390/physics7040051

physics

MDPI

Article

Reinterpretation of Fermi Acceleration of Cosmic Rays in Terms of Ballistic Surfing Acceleration in Supernova Shocks

Krzysztof Stasiewicz

Space Research Centre, Polish Academy of Sciences, Bartycka 18A, 00-716 Warsaw, Poland; kstasiewicz@cbk.waw.pl

Abstract

The applicability of the first-order Fermi mechanism—a cornerstone of the diffusive shock acceleration (DSA) model—in explaining the cosmic ray spectrum is reexamined in light of recent observations from the Magnetospheric Multiscale (MMS) mission at Earth's bow shock. It is demonstrated that the Fermi and DSA mechanisms lack physical justification and should be replaced by the physically correct ballistic surfing acceleration (BSA) mechanism. The results show that cosmic rays are energized by the convection electric field during ballistic surfing upstream of quasi-perpendicular shocks, independently of internal shock processes. The spectral index of cosmic rays is determined by the magnetic field compression and shock geometry: the acceleration is strongest in perpendicular shocks and vanishes in parallel shocks. The BSA mechanism reproduces the observed spectral indices, with $s = -2.7$ below the knee at 10^{16} eV and $s = -3$ above it. It is suggested that the spectral knee may correspond to particles whose gyroradii are comparable to the characteristic size of shocks in supernova remnants. The acceleration time to reach the knee energy, as predicted by the BSA, is in the order of 500 years.

Keywords: shock waves; acceleration of particles; cosmic rays; supernova remnants

Received: 27 June 2025
Revised: 9 September 2025
Accepted: 10 September 2025
Published: 16 October 2025

Citation: Stasiewicz, K. Reinterpretation of Fermi Acceleration of Cosmic Rays in Terms of Ballistic Surfing Acceleration in Supernova Shocks. *Physics* **2025**, *7*, 51. https://doi.org/10.3390/physics7040051

1. Introduction

Cosmic rays exhibit a power-law energy distribution, K^s, with a spectral index of $s \approx -2.7$ below the knee at an energy of $K \approx 5 \times 10^{15}$ eV and a steeper slope of $s \approx -3$ above the knee and below the ankle at 5×10^{18} eV [1–3]. Understanding the origin of this spectrum and the acceleration mechanisms capable of operating at such high energies remains crucial yet not fully resolved, problem in astrophysics. Enrico Fermi [4] proposed that the cosmic ray spectrum can arise from ions accelerated through repeated reflections from magnetic clouds in the interstellar medium—a process known as second-order Fermi acceleration. In contrast, first-order Fermi acceleration is now commonly regarded as the primary mechanism responsible for cosmic ray formation, operating through the process of diffusive shock acceleration (DSA) [5–8].

The recently launched Magnetospheric Multiscale (MMS) mission [9], consisting of four satellites flying through the Earth's bow shock, has provided the most accurate measurements of collisionless shocks to date. The MMS satellites occasionally operate with separation distances as small as 20 km, which is less than the thermal proton gyroradius of about 100 km. In this mission, the electric (**E**) and magnetic (**B**) fields are measured over a frequency range from 0 to 4 kHz, covering the ion and electron cyclotron frequencies as well as the ion plasma frequency. Particle distribution functions are recorded with a time resolution of 30 ms for electrons and 150 ms for ions.

Based on MMS data, it has been established that thermalization, heating, and acceleration of ions and electrons in collisionless shocks are governed by four key plasma processes—transit time thermalization (TTT), stochastic wave energization (SWE), quasi-adiabatic heating (QAH), and ballistic surfing acceleration (BSA)—all of which are further explained in this paper. While shocks are inherently complex and involve numerous additional acceleration processes, the four mechanisms listed appear to be the dominant pre-acceleration channels for high-energy particles and are consistently observed during every shock crossing by the MMS satellites. Understanding these processes in Earth's bow shock can provide insight into more powerful astrophysical shocks, such as those generated by supernova explosions, which are likely responsible for the acceleration of cosmic rays.

The TTT and SWE processes are stochastic in nature and associated with deterministic chaos. They depend on sufficiently strong gradients in the magnetic and electric fields, which lead to the randomization of particle orbits and enable efficient heating when stochastic criteria are met [10]. TTT thermalizes streaming ions via magnetic field gradients within a fraction of a gyroperiod, without requiring waves, instabilities, or anomalous collisions. In contrast, SWE is driven by sufficiently strong electric field gradients generated by plasma instabilities inside shocks and accelerates protons to energies of several hundred keV [11,12]. SWE acting on electrons is responsible for both heating and the formation of shell, ring, and flat-top electron distributions [13].

The QAH mechanism operates on particles for which the first adiabatic invariant is conserved ($v_\perp^2/B =$ constant, where $v_\perp$ denotes perpendicular velocity), a condition that requires the particle gyroradius r_c to be much smaller than the shock width, defined as $D \equiv B|\nabla B|^{-1}$. In shocks, this condition typically applies only to electrons. As a result, the perpendicular electron temperature varies as $T_\perp \propto B^{1+\alpha}$, where α quantifies the departure from perfect adiabaticity [14]. In quasi-perpendicular shocks, α is typically around $-1/3$, while positive values of α indicate additional heating of electrons by SWE.

BSA operates on particles with a gyroradius $r_c > D$, applying to superthermal ions with gyration energies greater than a hundred eV [10] and to mildly relativistic electrons with energy exceeding 180 keV. It bears a resemblance to the shock drift acceleration (SDA) previously discussed by various authors [15–17] and to shock surfing acceleration (SSA), where low-energy particles drift along the shock front due to surface waves [18–20].

In the processes of SSA, SDA, and BSA, energization occurs due to particle motion along the convection electric field. However, BSA takes place outside the shock, where particles with large gyroradii ($r_c \gg D$) engage in ballistic surfing in uniform fields and experience neither field gradients nor wave effects. In contrast, SDA implies ∇B drift acceleration, which occurs within the shock, and is equivalent to QAH for particles with $r_c < D$ [14].

Plasma can also be effectively heated by waves at resonance frequencies, such as the cyclotron, lower hybrid, upper hybrid, and plasma frequencies. Although resonant heating is observed, it does not appear to play a significant role in the acceleration of high-energy particles at shocks.

This raises the question of how the Fermi/DSA mechanism relates to the processes commonly observed at the Earth's bow shock. Section 2 examines the heating of energetic ions in a model shock in search of the signatures of Fermi acceleration. It is found that first-order Fermi acceleration lacks a rigorous physical foundation, whereas BSA provides a more accurate description of the acceleration process. Moreover, it is shown that the cosmic ray spectrum, including the presence of the knee, can be explained entirely by the BSA mechanism.

2. Ballistic Surfing Acceleration

To understand acceleration of high-energy particles, let us consider motion of test particles with the velocity v to be considerably larger than the thermal velocity v_{Ti} of ions that sustain the shock. The trajectories of particles with a rest mass of m_0 and charge of q are described by the momentum equation

$$\frac{\mathrm{d}\mathbf{p}}{\mathrm{d}t} = q(\mathbf{E} + \mathbf{v} \times \mathbf{B}), \tag{1}$$

where $\mathbf{p} = \gamma m_0 \mathbf{v}$, $\gamma = (1 - v^2/c^2)^{-1/2}$, and c is the speed of light. The kinetic energy gain of a particle, as implied by this equation, is given by

$$\Delta K = q \int \mathbf{E} \cdot \mathbf{v}\, dt. \tag{2}$$

In this paper, the shock reference frame is utilized in a geometry where the $\hat{\mathbf{x}}$ axis points in the opposite direction to the shock normal, $\hat{\mathbf{y}}$ is aligned with the convection electric field, and the magnetic field lies in the $[B_{x0}, 0, B_z(x)]$ plane. The model shock is described in [10] and represents a magnetic ramp in the form of $B_z \propto \tanh(x/D)$ with compression of $c_B = B_d/B_u$ between the downstream and upstream values. A normal component, B_{x0}, defines the upstream field angle, $\cos\eta = B_{x0}/B_u$, relative to $\hat{\mathbf{x}}$.

There are three types of electric fields that determine the particle dynamics and energization processes in a shock frame: $\hat{\mathbf{y}}E_y$—the convection field, constant across one-dimensional structures; $\hat{\mathbf{x}}E_S(x)$—the cross-shock electric field, maintained by the electron pressure gradient; and $\tilde{\mathbf{E}}(\mathbf{r}, t)$—the wave electric field. In the reference frame moving with the convection velocity, E_y vanishes; however, the magnetic field in a moving shock varies with the time, giving rise to an inductive electric field, $\nabla \times \mathbf{E} = -\partial \mathbf{B}/\partial t$, which can accelerate particles. Magnetic turbulence is not included in this shock model, but can be incorporated similarly to electrostatic waves. It is expected to contribute to the isotropization of particle distributions and scattering of particles back to the shock.

The parameters that are used in the model are as follows: the upstream sonic Mach number is $M = V_u/v_{Ti} = 8$, the ratio of the thermal ion gyroradius r_{ci} to the width of the shock ramp is $r_{ci}/D = 1$, and the compression is $c_B = 4$. The stochastic TTT parameter is set to $\chi_B = 8$ and the stochastic parameter for the cross-shock electric field to $\chi_S = 1.5$; see [10] for definitions.

Two ions were injected into an oblique shock, $\eta = 85°$, at $x = -40$ in units of the shock width, and then differential equations were used as described in Ref. [10]. The integration was performed using a standard MATLAB-R2024 routine with automatic step control to ensure a relative accuracy of 10^{-6}. Figure 1a shows the ion trajectories in plane (x, y). The initial velocity consists of the $\mathbf{E} \times \mathbf{B}$ drift normalized by the upstream thermal speed, $\mathbf{u}_{\mathbf{E}\times\mathbf{B}} = \mathbf{V}_{\mathbf{E}\times\mathbf{B}}/v_{Ti}$, with additional velocities being $u_x = +20$ (blue) and $u_y = -20$ (red). Figure 1b shows the total kinetic energies, u^2, of the ions along their respective trajectories, Figure 1c shows the gyration energies only, $(\mathbf{u}_\perp - \mathbf{u}_{\mathbf{E}\times\mathbf{B}})^2$, and Figure 1b shows $u_\parallel^2$. An adiabatic projection of the initial perpendicular energy of the red ion is shown as the black curve $b(x)u_{0\perp}^2$, where $b(x) = B(x)/B_u$. Both ions behave non-adiabatically and do not follow the adiabatic projection. One observes that the blue ion makes three crossings of the shock at $x = 0$, while the red ion makes seven crossings before being transmitted downstream. Each crossing is associated with an increase in the gyration energy, as seen in Figure 1c.

The kinetic energy in Figure 1b correlates with particle motion in the $\pm y$ direction along the electric field E_y, as seen in Figure 1a. This evident acceleration process has previously been associated with shock drift acceleration [15–17]. However, this termi-

nology is misleading, as the acceleration occurs outside the shock, whereas SDA relies on ∇B drift, which operates within the shock ramp. The term ballistic surfing acceleration (BSA), introduced in Ref. [10], is more appropriate, since particles accelerated by surfing in a gradient-free region are unaware of the shock's presence and therefore cannot undergo SDA.

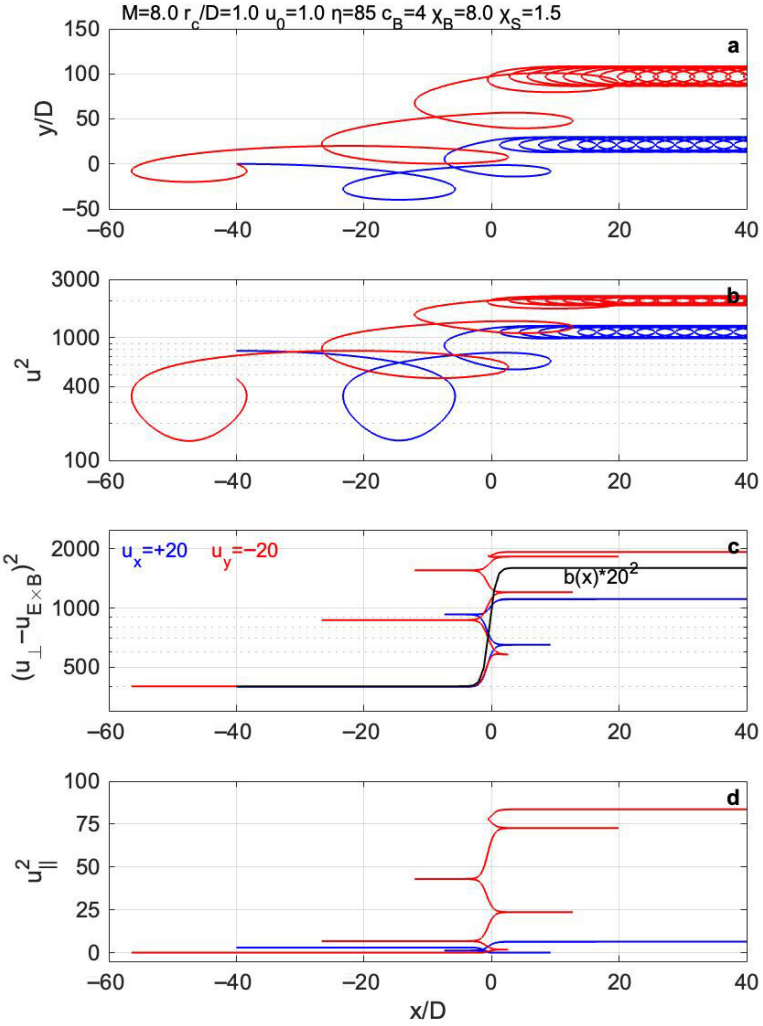

Figure 1. Ion trajectories and heating due to TTT and BSA in an oblique shock with a shock angle of $\eta = 85^\circ$, $\chi_B = 8$, a cross-shock electric field of $\chi_S = 1.5$, a compression of $c_B = 4$, and a thickness ratio of $r_{ci}/D = 1$, without waves. (**a**) Trajectories of two ions injected at $x = -40$ with a sonic Mach number of $M = 8$ and the additional velocities $u_x = +20$ (blue) and $u_y = -20$ (red) in units of the upstream ion thermal velocity v_{Ti}. (**b**) Total kinetic energies of ions along their respective trajectories. (**c**) Thermal (gyration) energies of ions along their trajectories. The black curve shows theoretical adiabatic heating for the shock profile given by $b(x) \equiv B(x)/B_u$. (**d**) Parallel energies of ions along their trajectories. Typical values upstream of the bow shock are $T_i \approx 20$ eV, $v_{Ti} \approx 60$ km s^{-1}, $r_{ci} \approx 100$ km, and $B_u \approx 5$ nT. See text for more details.

By decreasing the shock angle to $\eta = 70^\circ$ in Figure 2, one finds the red ion being reflected back into the upstream region. Such particle reflections become more common at smaller shock angles, η, but those reflections are not caused by the magnetic mirror force—which does not affect particles with large gyroradii ($r_c > D$)—nor by the cross-shock potential. The latter has a normalized energy of $e\Delta\Phi/T_{eu} \approx 2(c_B - 1) = 6$, where $T_{eu} \approx T_{iu}$. This is small even for cold ions with an energy of $u^2 = M^2 = 64$ (see [10]) and negligible for

high-energy ions with $u^2 \sim 1000$, as in the present simulations. Moreover, the cross-shock potential energy does not accumulate over time—it cancels out after each gyration around the shock.

The transfer of energy into parallel motion, as shown in Figure 2d, is not related to the cross-shock electric field, which has a parallel component, $E_{\parallel} = E_S(x)\cos\eta$, as the patterns remain the same when E_S is set to zero. Instead, it results from the TTT process, which is associated with the changing direction of the magnetic field and also governs particle reflections.

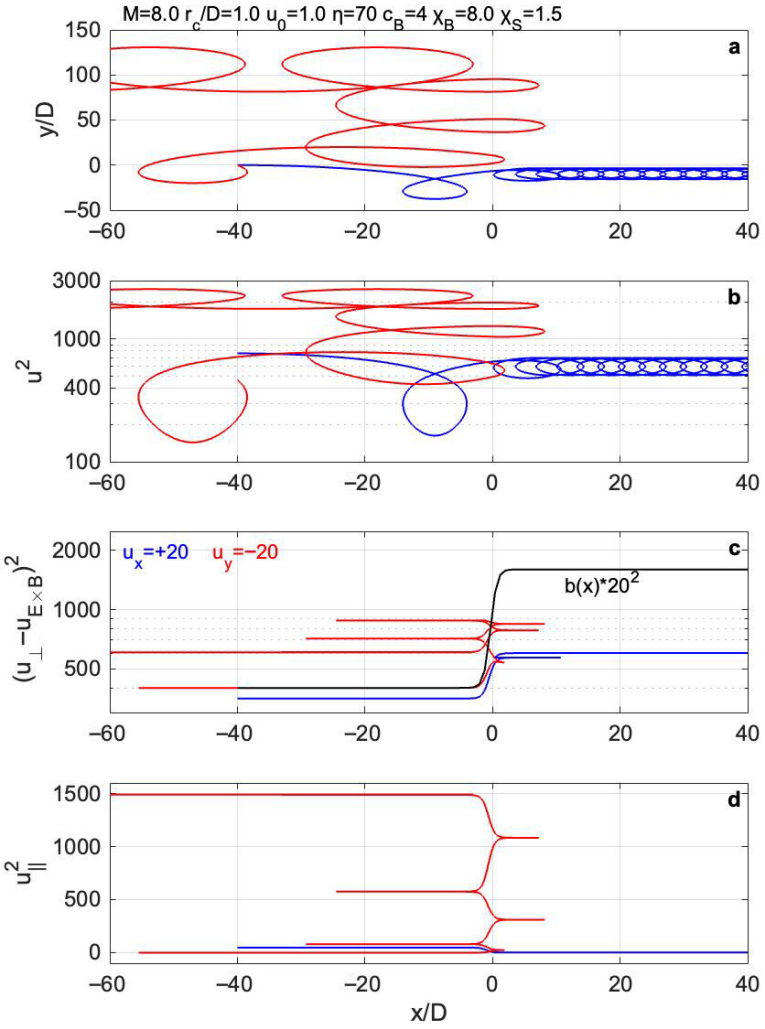

Figure 2. BSA and TTT of ions as in Figure 1 but for a shock angle of $\eta = 70°$. The red ion is reflected upstream. The ion gyration energy is $u_{\perp}^2 = 400$, and the drift energy $M^2 = 64$ at the starting position of $x = -40$.

Most studies mistakenly interpret cyclotron turning points—where a particle's velocity, v_x, is reversed—as shock reflections. Cyclotron turning occurs periodically—once every gyroperiod—whereas true shock reflections, as well as transmissions, are singular events that occur only once. Turning points occur cyclically at various locations, depending on the initial conditions, and are unrelated to magnetic mirroring.

Contrary to a common belief, high-energy particles are not reflected by shocks or magnetic field gradients. Instead, the particles traverse these regions with only minor changes in their velocity direction, as illustrated in Figures 1 and 2. Similarly, magnetic turbulence outside a shock—which has a much smaller amplitude than the shock itself—does not

reflect particles but merely causes even smaller deflections in their trajectories. After a number of such deflections, facilitated by the TTT process, some transmitted or reflected particles may acquire a parallel velocity component that enables them to return to the shock and re-engage in the acceleration process.

As shown in Figures 1b and 2b, each cyclotron turn into the upstream direction—commonly interpreted as a "reflection"—is consistently accompanied by a loss rather than a gain in particle energy. This contradicts Fermi's original concept of cosmic ray acceleration via head-on collisions with regions of enhanced magnetic field strength [4]. The discrepancy arises from his reliance on acceleration through magnetic mirroring under conservation of adiabatic invariants, a mechanism not applicable to cosmic ray particles with large gyroradii. Moreover, all the transitions of high-energy particles through the shock region ($|x| < D$) occur without significant changes in the kinetic energy (u^2), directly challenging the central premise of the DSA model, which attributes acceleration to shock crossings. This suggests that the Fermi and DSA mechanisms may not represent physical reality.

3. Results

3.1. BSA and Formation of the Cosmic Ray Spectrum

As shown in Section 2, energetic particles are accelerated outside the shock via the BSA process, which is driven by the convection electric field E_y, rather than by shock reflections or transitions, as postulated in the Fermi and DSA models. The BSA process is elucidated in Figure 3, where it can be observed that ions moving in the $+y$ direction in the upstream part of the orbit gain kinetic energy ($qE_y v_y > 0$), while those moving in the $-y$ direction in the downstream part lose energy ($qE_y v_y < 0$). Because $B_d > B_u$, the downstream gyroradius r_{cd} is smaller than the upstream gyroradius r_{cu}, resulting in a net energy gain for the particles after each gyroperiod, irrespective of which side the particles enter the shock from.

Within the shock ramp denoted by vertical lines at $x = \pm D$, the particles experience gyrocenter drifts induced by ∇B and are subjected to combined convection, cross-shock, and wave electric fields, $\mathbf{E} = \hat{\mathbf{y}}E_y + \hat{\mathbf{x}}E_S(x) + \tilde{\mathbf{E}}$. The expression for the total energy gain after a full rotation around the shock generally consists of four terms:

$$\Delta K = \int_{|x|\geq D}^{\text{BSA}} qE_y v_y dt + \int_{|x|<D}^{\text{SDA}} qE_y v_y dt + \int_{|x|<D}^{\text{C-S}} qE_S v_x dt + \int_{|x|<D}^{\text{SWE}} q\tilde{\mathbf{E}} \cdot \mathbf{v}\, dt, \tag{3}$$

where the first term corresponds to the BSA outside the shock ramp, the second to the SDA within the ramp, the third to acceleration induced by the cross-shock (C-S) electric field, and the fourth to SWE and other wave-driven mechanisms. Waves outside shocks generally have amplitudes below the stochastic threshold and are therefore assumed to contribute negligibly to particle acceleration.

The BSA term provides the dominant contribution to the acceleration of high-energy particles, while the effects of the SDA, C-S potential, SWE, and other processes within the shock are negligible due to the extremely short interaction time relative to the gyroperiod. For example, a cosmic ray proton with a kinetic energy of $K = 10^{12}$ eV undergoes only about 0.3 ms of acceleration within a shock with a width of $D = 100$ km, compared to approximately 10 h of continuous acceleration induced by the convection electric field E_y via BSA in an upstream magnetic field of $B_u = 1$ nT. Conversely, for particles with small gyroradii ($r_c < D$), TTT, SWE, and QAH/SDA serve as the primary heating and acceleration mechanisms, while BSA is not applicable.

After one gyration across the shock, the energy gain corresponding to the first term in Equation (3) is $\Delta K \approx 2qE_y(r_{cu} - r_{cd})$, as illustrated in Figure 3. For relativistic particles with a kinetic energy of $K \approx pc$ and gyroradius of $r_c = p_\perp/qB$, the energy gain is

$$\Delta K \approx 2qE_y \frac{1}{\pi}\int_0^\pi (r_{cu} - r_{cd}) \sin\theta \, d\theta = g(1 - c_B^{-1})\frac{V_u}{c}K, \tag{4}$$

where $V_u = E_y/B_u$ is the upstream convection velocity, $g = 1$, and the integral is the average over the pitch angles, assuming an isotropic distribution. The geometric factor $g \lesssim 1$ is retained here to account for averaging over incident angles and to include a dependence on the shock angle η, which cannot be determined analytically.

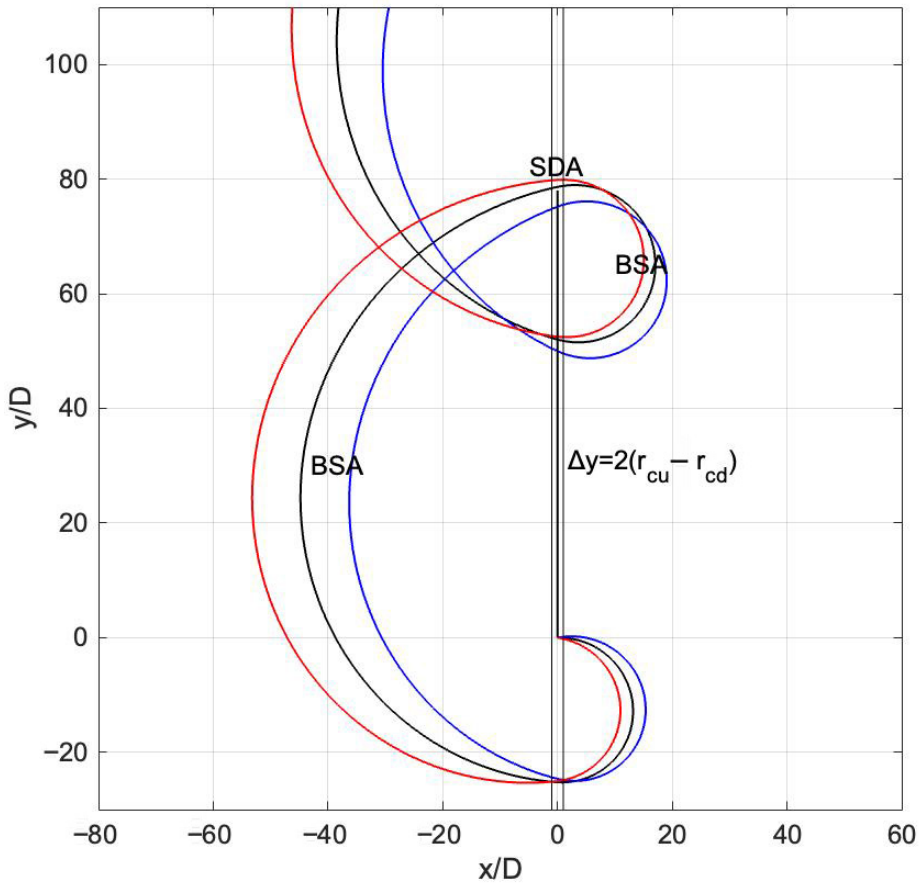

Figure 3. An explanation of ballistic surfing acceleration. Three ions with a perpendicular velocity of $v_\perp = 50v_{Ti}$ are injected at incident angles of 0° (black), +10° (blue), and −10° (red) into the perpendicular shock located at position $x = 0$. The parameters are set as follows: $c_B = 4$, a Mach number of $M = 3$, $r_{ci}/D = 1$, and a cross-shock electric field of $\chi_S = 1.5$. The energy gain after one gyration across the shock is $\Delta K \approx 2qE_y(r_{cu} - r_{cd})$, which leads directly to Equation (4). TTT, SDA, and SWE occur within the ramp denoted by vertical lines, where $|x|/D < 1$, while BSA operates in the gradient-free zone where $|x|/D > 1$. See text for more details.

Equation (4) is alike the expression derived for the DSA where high-energy particles undergo multiple shock transitions. The energy difference per cyclic encounter, averaged over an isotropic initial distribution, is known as the first-order Fermi acceleration, given by

$$\Delta K_F = \frac{4}{3}\left(1 - c_N^{-1}\right)\frac{V_{xu}}{c}K. \tag{5}$$

Equation (5) was derived in Ref. [5] (see also the monographs [7,8]) from the difference in the particle energy between the upstream and downstream inertial frames, characterized

by the normal velocity ratio $V_{xu}/V_{xd} = n_d/n_u \equiv c_N$, as required by the continuity equation. Here, c_N denotes the density compression ratio, typically set to the standard value $c_N = 4$, according to the Rankine–Hugoniot relations [21]. Note that Equation (4) vanishes in parallel shocks because $V_u = V_{xu} \sin\eta = 0$ for $\eta = 0$, whereas Equation (5) is independent of η. This distinction—together with the difference between c_B and c_N—makes the two expressions fundamentally different. The latter is shown to be non-physical in Section 4.

Equation (4) implies that the particle energy after completing a full gyration around the shock is

$$K_1 = hK_0; \quad h = 1 + g(1 - c_B^{-1})V_u/c. \tag{6}$$

By analogy with the DSA scenario, it is assumed here that particles transmitted downstream may be scattered back to the shock by turbulence, while particles reflected upstream can either be deflected and convected back or encounter another shock front.

Here, the standard analytical approach is applied as outlined by Tony Bell [5] and described also in monographs [7,8]. Let P be the probability that particles remain in the shock region after one interaction or gyration. Then, after j interactions, there are $N = N_0 P^j$ particles with energies of $K = K_0 h^j$. Eliminating j gives $N/N_0 = (K/K_0)^{\ln P/\ln h}$, where N is the number of particles that have reached an energy of K and can be further accelerated. Using a universal, process-independent expression for the probability derived from the flux continuity,

$$P \approx 1 - 4V_{xd}/c, \tag{7}$$

one obtains the spectrum of cosmic rays predicted by the BSA model:

$$\frac{\mathrm{d}N}{\mathrm{d}K} \propto K^s. \tag{8}$$

Here, the spectral index s is defined as

$$s = \frac{\ln P}{\ln h} - 1 \approx -\left(\frac{4(g\sin\eta)^{-1}}{c_B - 1} + 1\right) = -\left(\frac{4}{c_B' - 1} + 1\right), \tag{9}$$

where the effective compression $c_B' = g\sin\eta(c_B - 1) + 1$ is introduced. The observed spectral index $s = -2.7$ is obtained from this equation for the standard compression of $c_B = 4$ and $g\sin\eta = 0.78$ or an effective $c_B' = 3.6$, while a steeper spectrum, $s = -3$, observed above the knee energy, corresponds to $g\sin\eta = 0.66$ or an effective $c_B' = 3$. The acceleration efficiency depends on the shock angle and is strongest for perpendicular shocks ($\eta = 90°$), producing the flattest spectrum with a spectral index of $s_{\max} = -2.3$ for $c_B = 4$ and $g\sin\eta = 1$. The efficiency decreases with a decreasing η and vanishes for parallel shocks ($\eta = 0°$), where $s \to -\infty$.

Using the expression $h_F = 1 + \frac{4}{3}(1 - c_N^{-1})V_{xu}/c$ from Equation (5), one recovers the known DSA model [5,7,8],

$$s_F = \frac{\ln P}{\ln h_F} - 1 = -\left(\frac{3}{c_N - 1} + 1\right), \tag{10}$$

which, for $c_N = 4$, yields a spectral index of $s_F = -2$, independent of the shock angle and significantly different from the observed value of -2.7. The physical validity of this expression is questioned in Section 4.

3.2. Acceleration in Quasi-Parallel Shocks: MMS Observations

Quasi-parallel shocks do not have a well-defined front, as seen in quasi-perpendicular shocks. Instead, such shocks break up into a myriad of spatially distributed magnetic pulsations (shocklets), characterized by strong compressions of the density and mag-

netic field ($c_N \approx c_B \lesssim 10$) with a perpendicular spatial scale of $L_\perp \approx 3r_{ci}$ and a parallel length of $L_\parallel \approx 3L_\perp$ [12].

For strictly parallel shocks ($E_y \approx 0$), the first two terms in Equation (3) vanish, leaving only the cross-shock electric field and wave energization as mechanisms for increasing the particle energy. The C-S electric field, associated with electron pressure gradients in shocklets, consists of oppositely directed bipolar structures that exert no net effect on the high-speed particles traversing them. However, when the electric field gradients exceed the stochastic threshold [10], C-S acceleration transitions into the SWE mechanism. Consequently, the dominant energization is provided by the last term in Equation (3).

The energization $\int q\tilde{\mathbf{E}} \cdot \mathbf{v}dt$ by waves outside shocks can at most equal the wave potential, which is negligible for high-energy particles regardless of the wave mode. Waves measured inside shocks have amplitudes of $\tilde{E} \approx 20$–200 mV m^{-1} in various modes over a frequency range of 0–1 kHz, significantly exceeding that of the convection field, $E_y \approx 1$–5 mV m^{-1}. As shown in Refs. [10–12], the waves observed in Earth's bow shock far exceed the threshold for stochastic heating, accelerating ions via SWE to energies of $K_{\mathrm{SWE}} = m(\tilde{E}_\perp/B)^2/2$ and typically reaching a few hundred keV for protons. MMS observations confirm that quasi-parallel shocks produce high-energy ions only up to 300 keV, thereby validating the SWE mechanism. This natural limitation implies that parallel shocks are unlikely to contribute to the proton spectrum above 1 MeV, consistent with Equations (4) and (9), which show that BSA vanishes in parallel shocks.

3.3. The Position of the Knee Energy

Although BSA functions effectively at an arbitrarily high energy, the acceleration in the upstream region is canceled out by deceleration in the downstream region as the diameter of the orbit on the compressed side approached the shock length L; see Figure 3. The condition $2r_{cd} \approx L$, together with $K \approx pc$, $r_c = p_\perp/qB$, then results in a knee in the spectrum located at an energy of

$$K_L \approx \frac{qc}{2}\langle LB_d \rangle. \tag{11}$$

The observed distribution of supernova remnant sizes ranges from 1 pc (of 3×10^{16} m) to 200 pc [22]. The observed knee energy, $K_L \approx 5 \times 10^{15}$ eV, is derived from Equation (11) for $\langle LB_d \rangle \approx 1$ nT pc, which may correspond to, for example, $B_d \approx 1$ nT on the inner (compressed) side of a spherically expanding supernova shock and $L \approx 1$ pc. Importantly, Equation (11) is independent of the shock velocity and the particle mass, which underscores its universality.

However, even particles with gyroradii considerably larger than the shock length can undergo further acceleration. This situation may arise when downstream flows become stagnant in the shock frame ($V_d \sim 0$), causing the electric field to vanish at some distance from the shock, $E_{yd} \sim 0$. Particles gyrating in the downstream region then avoid deceleration, as shown in Figures 1b and 2b, while still being accelerated in the upstream region according to $\mathrm{d}K/\mathrm{d}t = qE_y v_y > 0$. This process may account for cosmic ray energies up to the ankle at 5×10^{18} eV in shocks shorter than the gyroradius. The observed spectral index in this energy range, $s = -3$, can be reproduced using Equation (9) for an effective compression of $c'_B = 3$.

3.4. The Acceleration Time to the Knee Energy

The initial heating of cold ions in shocks is governed by two stochastic mechanisms, TTT and SWE, as illustrated in Figure 4 of Ref. [10]. In this case, streaming protons with an initial temperature of $T_i \approx 20$ eV are first thermalized by TTT, then accelerated by SWE, and finally reach about 400 $T_i \approx 8$ keV through BSA within a single gyroperiod. In narrow quasi-perpendicular shocks these ions are rapidly convected downstream, limiting

their energy gain to about 20 keV. By contrast, in spatially extended quasi-parallel shocks, prolonged interactions with electric field turbulence can raise the proton energies to the K_{SWE} limit of a few hundred keV, as discussed in Section 3.2.

Ions and electrons with large gyroradii continue accelerating by gyrating around quasi-perpendicular shocks. Let us assume that protons start the BSA process with an energy of $K_0 = 10$ keV and that the shock parameters are $c_B = 4$ and $V_u = 10{,}000$ km s^{-1}. Using the exact form of Equation (4) with the kinetic energy defined as $K \equiv (m_0^2c^4 + p^2c^2)^{1/2} - m_0c^2$, one finds that protons reach the knee at $K = 5 \times 10^{15}$ eV after 657 BSA interactions, assuming no energy losses. For a higher shock speed of $V_u = 20{,}000$ km s^{-1}, the final energy may be reached after 334 BSA interactions. For protons moving in the average magnetic field of $\langle B \rangle = 1$ nT, the net acceleration time of 657 (334) gyroperiods corresponds to 443 (226) years of sidereal time, accounting for time dilation during each gyroperiod.

4. Evidence for the Non-Physicality of the Fermi and DSA Mechanisms

Although Fermi acceleration and the DSA model are widely accepted frameworks for explaining cosmic ray acceleration, they lack a rigorous physical foundation, as indicated earlier, and should instead be replaced by the BSA model, which is well grounded in fundamental physics. The six arguments outlined below challenge the physical validity of the Fermi and DSA mechanisms as viable models of particle acceleration.

1. The Fermi and DSA formulations neglect the essential role of the electric field in particle energization. Instead, they attribute energy gains either to shock transitions—where, in reality, significant acceleration does not occur—or to particle reflections in regions of increasing magnetic field strength, which are in fact natural cyclotron turns that lead to energy loss. These issues, discussed in detail in Section 2, raise questions about the physical validity of both mechanisms.
2. Proponents of the DSA mechanism argue that particles gain the same amount of energy during both upstream-to-downstream and downstream-to-upstream shock transitions, resulting in the factor of $\frac{4}{3}$ being used in Equation (5). However, this claim is physically unfounded and inconsistent with the fundamental equations of electrodynamics, as demonstrated in Figures 1b, 2b, and 3 from which one can immediately find that particles consistently lose energy on the downstream side, gain energy only by surfing on the upstream side, and experience no significant energy change during shock crossings, regardless of their direction.
3. The first-order Fermi Equation (5), which forms the foundation of the DSA model (10), was derived from the energy transformation between upstream and downstream inertial frames with a velocity ratio of $V_{xu}/V_{xd} = c_N$. This transformation has been interpreted—without physical justification—as representing particle energization by Bell [5] and in subsequent studies including monographs [7,8]. However, physical energization—rigorously defined by Equations (2) and (3)—must be evaluated within a single reference frame, and correctly leads to the BSA Equation (4), fundamentally different from Equation (5).
4. A superficial similarity between the correct Equation (9) and the incorrect Equation (10) helps explain why the DSA model has gained enduring recognition, despite its fundamentally flawed physical basis. This acceptance may be due to the commonly observed relation $n \propto B$ in shocks, which gives $c_N \approx c_B$. Consequently, the circumstantial correlation between the spectral index and the particle energy gain with c_N has been mistaken for a genuine physical effect, whereas the true dependence is on c_B.
5. The symbols in Equations (1) and (2) indicate that any physically valid energization formula can depend only on E, B, v_0, the time, and the system size L. It should not depend on the plasma density or parallel bulk velocity, since these quantities neither

appear in the governing equations nor can they be constructed from the available physical parameters. For this reason, Equation (5), derived by Bell [5] specifically for parallel shocks ($E_y = 0$) and based solely on parallel flows (V_{xu}) and density compression ($V_{xu}/V_{xd} = c_N$), is a priori an invalid expression for the energy gain, thereby invalidating DSA. Remarkably, this equation has become a cornerstone of the DSA model, even though it contains no electric fields and thus makes energization a priori impossible. By contrast, the BSA Equations (4) and (11) satisfy the requirement for physical consistency.

6. There are numerous simulation studies (e.g., [23–30]) reporting on an apparent agreement with the DSA model. This apparent consistency arises from the numerical similarity between the correct BSA Equations (4) and (9) and the commonly used—but physically incorrect—DSA Equations (5) and (10) for shock compression ratios of 3–4. Under these conditions, both models produce comparable spectral slopes, which may mislead those unaware of the non-physical basis of the DSA model into interpreting their results as supporting its validity. However, the general energization Equation (3), contains no term attributable to Fermi or DSA processes, indicating that these mechanisms may not exist in physical reality. Nevertheless, the studies [23–30] appear to be fully consistent with the BSA model, which should be explicitly acknowledged by the authors.

5. Conclusions

1. This paper clarifies several physical misconceptions that originated in the early years of shock research, when high-quality in situ measurements were not yet available. First, it straightforwardly demonstrates that widely accepted mechanisms—such as Fermi acceleration and diffusive shock acceleration—lack a rigorous physical foundation. It also highlights that shock drift acceleration, which specifically refers to the ∇B drift of gyrocenters within the shock ramp, has been inappropriately extended in some studies to describe processes occurring outside shocks, such as ballistic surfing acceleration.
2. Cosmic rays are shown to be accelerated by the convection electric field E_y during ballistic surfing upstream of quasi-perpendicular shocks, independently of the processes and field gradients inside the shock. The BSA mechanism renders obsolete three models that lack physical justification: Fermi acceleration, DSA, and also SDA when applied to particles with large gyroradii.
3. The spectral index in the BSA model is determined by the shock compression ratio c_B and the shock angle η. It is shown to accurately reproduce the observed index of $s \approx -2.7$ below the knee energy, as well as the steeper spectrum of $s \approx -3$ above the knee. By varying the shock angle η, the BSA mechanism is shown to be able to reproduce any spectral index, s, within the range $[-\infty, -2.3]$, while keeping the compression fixed at $c_B = 4$ and without invoking propagation effects.
4. The BSA model is found to predict reduced acceleration when the gyroradius approaches the shock length, defining the knee energy using Equation (11). To reach the knee energy of 5×10^{15} eV, a proton starting from 10 keV in a collisionless environment requires only 657 BSA interactions (gyroperiods) in shocks moving at $V_u = 10,000$ km/s. This corresponds to 443 years of sidereal time in an average magnetic field of $\langle B \rangle = 1$ nT, assuming no energy losses.
5. It is argued that energization in shocks caused by a combination of TTT, QAH/SDA, and SWE processes occurs continuously from initial gyration energies near zero, reaching several hundred keV for ions in quasi-parallel shocks. Beyond this range, further acceleration occurs exclusively via BSA during gyrations around quasi-perpendicular shocks, reaching energies of 10^{16} eV and beyond in sufficiently extended shocks ($L \approx 1$ pc). Cosmic ray acceleration is found to be the most efficient in perpendicular shocks and negligible in parallel shocks.

Funding: This work was supported by the Narodowe Centrum Nauki (NCN), Poland, through grant No. 2021/41/B/ST10/00823.

Data Availability Statement: The mathematical shock model used to create Figures 1–3 was published at https://doi.org/10.1093/mnrasl/slad071.

Conflicts of Interest: The author declares no conflicts of interest.

Abbreviations

BSA	ballistic surfing acceleration
C-S	cross-shock
DSA	diffusive shock acceleration
QAH	quasi-adiabatic heating
SDA	shock drift acceleration
SSA	shock surfing acceleration
SWE	stochastic wave energization
TTT	transit time thermalization

References

1. Hillas, A.M. The origin of ultra-high-energy cosmic rays. *Annu. Rev. Astron. Astrophys.* **1984**, *22*, 425–444. [CrossRef]
2. Hillas, A.M. Can diffusive shock acceleration in supernova remnants account for high-energy galactic cosmic rays? *J. Phys. G* **2005**, *31*, R95–R131. [CrossRef]
3. Helder, E.; Vink, J.; Bykov, A.; Ohira, Y.; Raymond, J.; Terrier, R. Observational signatures of particle acceleration in supernova remnants. *Space Sci. Rev.* **2012**, *173*, 369–431. [CrossRef]
4. Fermi, E. On the origin of the cosmic radiation. *Phys. Rev.* **1949**, *75*, 1169–1174. [CrossRef]
5. Bell, A.R. The acceleration of cosmic rays in shock fronts—I. *Mon. Not. R. Astron. Soc.* **1978**, *182*, 147–156. [CrossRef]
6. Blandford, R.; Eichler, D. Particle acceleration at astrophysical shocks: A theory of cosmic ray origin. *Phys. Rep.* **1987**, *154*, 1–75. [CrossRef]
7. Vietri, M. *Foundations of High Energy Astrophysics*; The University of Chicago Press: Chicago, IL, USA, 2008. Available online: https://archive.org/details/foundationsofhig0000viet/ (accessed on 9 September 2025).
8. Longair, M.S. *High Energy Astrophysics*; University of Cambridge: Cambridge, UK, 2011. [CrossRef]
9. Burch, J.L.; Moore, R.E.; Torbert, R.B.; Giles, B.L. Magnetospheric Multiscale overview and science objectives. *Space Sci. Rev.* **2016**, *199*, 5–21. [CrossRef]
10. Stasiewicz, K. Transit time thermalization and the stochastic wave energization of ions in quasi-perpendicular shocks. *Mon. Not. R. Astron. Soc.* **2023**, *524*, L50–L54. [CrossRef]
11. Stasiewicz, K.; Eliasson, B.; Cohen, I.J.; Turner, D.L.; Ergun, R.E. Local acceleration of protons to 100 keV in a quasi-parallel bow shock. *J. Geophys. Res. Space Phys.* **2021**, *126*, e2021JA029477. [CrossRef]
12. Stasiewicz, K.; Kłos, Z. On the formation of quasi-parallel shocks, magnetic and electric field turbulence, and ion energisation mechanism. *Mon. Not. R. Astron. Soc.* **2022**, *513*, 5892–5899. [CrossRef]
13. Stasiewicz, K. Origin of flat-top electron distributions at the Earth's bow shock. *Mon. Not. R. Astron. Soc.* **2023**, *527*, L71–L75. [CrossRef]
14. Stasiewicz, K.; Eliasson, B. Electron heating mechanisms at the bow shock—Revisited with Magnetospheric Multiscale measurements. *Mon. Not. R. Astron. Soc.* **2023**, *520*, 3238–3244. [CrossRef]
15. Jokipii, J.R. Particle drift, diffusion and acceleration at shocks. *Astrophys. J.* **1982**, *255*, 716–720. [CrossRef]
16. Decker, R. Computer modeling of test particle acceleration at oblique shocks. *Space Sci. Rev.* **1988**, *48*, 195–262. [CrossRef]
17. Jones, F.C.; Ellison, D.C. The plasma physics of shock acceleration. *Space Sci. Rev.* **1991**, *58*, 259–346. [CrossRef]
18. Shapiro, V.D.; Lee, M.A.; Quest, K.B. Role of lower hybrid turbulence in surfing acceleration at perpendicular shocks. *J. Geophys. Res. Space Phys.* **2001**, *106*, 25023–25030. [CrossRef]
19. Lever, E.L.; Quest, K.B.; Shapiro, V.D. Shock surfing vs. shock drift acceleration. *Geophys. Res. Lett.* **2001**, *28*, 1367–1370. [CrossRef]
20. Hoshino, M.; Shimada, N. Nonthermal electrons at high Mach number shocks: Electron shock surfing acceleration. *Astrophys. J.* **2002**, *572*, 880–887. [CrossRef]
21. Kennel, C.F. Shock structure in classical magnetohydrodynamics. *J. Geophys. Res. Space Phys.* **1988**, *93*, 8545–8557. [CrossRef]
22. Badenes, C.; Maoz, D.; Draine, B.T. On the size distribution of supernova remnants in the Magellanic Clouds. *Mon. Not. R. Astron. Soc.* **2010**, *407*, 1301–1313. [CrossRef]
23. Kang, H.; Ryu, D. Diffusive shock acceleration at cosmological shock waves. *Astrophys. J.* **2013**, *764*, 95. [CrossRef]

24. Caprioli, D.; Spitkovsky, A. Simulations of ion acceleration at non-relativistic shocks. I. Acceleration efficiency. *Astrophys. J.* **2014**, *783*, 91. [CrossRef]
25. Giacalone, J. Diffusive shock acceleration of high-energy charged particles at fast interplanetary shocks: A parameter survey. *Astrophys. J.* **2015**, *799*, 80. [CrossRef]
26. Ohira, Y. Injection to rapid diffusive shock acceleration at perpendicular shocks in partially ionized plasmas. *Astrophys. J.* **2016**, *827*, 36. [CrossRef]
27. Ryu, D.; Kang, H.; Ha, J.H. A diffusive shock acceleration model for protons in weak quasi-parallel intracluster shocks. *Astrophys. J.* **2019**, *883*, 60. [CrossRef]
28. Cristofari, P.; Blasi, P.; Caprioli, D. Microphysics of diffusive shock acceleration: Impact on the spectrum of accelerated particles. *Astrophys. J.* **2022**, *930*, 28. [CrossRef]
29. Orusa, L.; Caprioli, D. Fast particle acceleration in 3D hybrid simulations of quasiperpendicular shocks. *Phys. Rev. Lett.* **2023**, *131*, 095201. [CrossRef]
30. Aerdker, S.; Merten, L.; Becker Tjus, J.; Walter, D.; Effenberger, F.; Fichtner, H. Numerical modeling of time dependent diffusive shock acceleration. *J. Cosmol. Astropart. Phys.* **2024**, *2024*, 068. [CrossRef]